East European Journal of Physics. 3. 413-423 (2023)
DOI:10.26565/2312-4334-2023-3-45 ISSN 2312-4334

# AB-INITIO STUDY OF STRUCTURAL, ELECTRONIC AND OPTICAL PROPERTIES OF ZnX (X = Te, S and O): APPLICATION TO PHOTOVOLTAIC SOLAR CELLS[†]

**Faiza Benlakhdar[a,*], Idris Bouchama[b,c], Tayeb Chihi[c,d], Ibrahim Ghebouli[c,d], Mohamed Amine Ghebouli[c], Zohra Zerrougui[e], Khettab Khatir[f], Mohamed Alam Saeed[g]**

[a]*Electronics Department, Faculty of Technology, University of Setif 1, 19000, Algeria*
[b]*Electronics Department, Faculty of Technology, University of Msila, Msila, 28000, Algeria*
[c]*Research Unit on Emerging Materials (RUEM), University Ferhat Abbas of Setif 1, Setif, 19000, Algeria*
[d]*Laboratory for Elaboration of New Materials and Characterization (LENMC), University of Ferhat Abbas, Setif 19000, Algeria*
[e]*Laboratory of Surfaces and Interfaces Studies Solid Materials (LESIMS), Department of Technology, Ferhat ABBAS Setif1 University, Setif, Algeria*
[f]*Department of Electrical Department, Faculty of Technology, University of Msila, Msila, 28000, Algeria*
[g]*Department of Physics, Division of Science & Technology, University of Education, Lahore, Pakistan*
**Corresponding author e-mail: benlakhdar228@gmail.com*
Received April 25, 2023; revised June 6, 2023 accepted June 7, 2023

The purpose of this research is to investigate the structural, electronic, and optical properties of ZnX compounds, particularly those with X = Te, S, and O, which have direct bandgaps that make them optically active. To gain a better understanding of these compounds and their related properties, we conducted detailed calculations using density functional theory (DFT) and the CASTEP program, which uses the generalized gradient approximation (GGA) to estimate the cross-correlation function. Our results for lattice modulus, energy bandgap, and optical parameters are consistent with both experimental data and theoretical predictions. The energy bandgap for all compounds is relatively large due to an increase in s-states in the valence band. Our findings suggest that the optical transition between (O - S - Te) - p states in the highest valence band and (Zn - S - O) - s states in the lowest conduction band is shifted to the lower energy band. Therefore, ZnX compounds (X = Te, S and O) are a promising option for optoelectronic device applications, such as solar cell materials.
**Keywords:** *ZnTe; ZnS; ZnO; CASTEP; DFT; Density of state; Optical properties*
**PACS:** 36.40.Cg, 87.15.Pc, 87.19.rf, 91.60.Pn, 14.60.Cd, 84.60.Jt, 82.47.Jk

## I. INTRODUCTION

Zinc monochalcogenides (ZnX: X = O, S, Se and Te) are considered the prototype of II-VI semiconductors and can crystallize in either the zinc-blende (z) or wurtzite (w) type structures. The ZnX-z phases are optically isotropic, while the ZnX-w phases are anisotropic, with c serving as the polar axis [1]. Due to their optical properties, ZnX phases are considered prime candidates for use in optical devices, such as visual displays, high-density optical memories, transparent conductors, solid-state laser devices, photodetectors, and solar cells [1]. Thus, understanding the optical properties of these materials is crucial in designing and analyzing ZnX-based optoelectronic devices [1]. ZnO, with a wide direct band-gap of approximately 3.37 eV at room temperature, is a typical semiconductor used for optoelectronic applications. It also possesses transparent properties in visible light and is non-toxic since zinc is abundant in the earth [2].

ZnS, ZnSe, and ZnTe are part of a family of IIB-VIA compounds that crystallize in the cubic zinc-blende structure at ambient pressure and have direct energy band-gaps [3]. These wide band-gap semiconductors are of significant interest since they are capable of emitting light even at room temperature [4]. Zinc Telluride (ZnTe) is of particular interest due to its low cost, high optical absorption coefficient, and suitability for use in PV applications [5]. It has also made extensive contributions to the field of microelectronics and optoelectronics applications [6]. Researchers have conducted various studies to investigate the electronic, structural, and dynamic properties of zinc-based semiconductors, such as Agrawal et *al.*, who used ab-initio to calculate these properties [7]. D. Bahri et *al.* investigated the structural, electronic, and optical properties of ZnTe cubic zinc-blende phase with the space group F-43m [8]. J. Serrano et *al.* used ab-initio to study the network dynamics of ZnO [9]. P. Walter et *al.* calculated the electronic energy band structures of ZnTe and ZnSe using the experimental pseudo-voltage method, which included spin-orbit coupling [10].

The focus of current research is on investigating the structural, electronic, and optical properties of ZnX (X = Te, S, and O) for potential photovoltaic applications, using the Density Functional Theory and GGA/PBE gradient approximation.

## II. COMPUTATIONAL DETAILS

In this research, we utilized the CASTEP software [11] to analyze the structural, electronic, and optical characteristics of ZnX compounds, where X denotes Te, S, and O. The compounds have a space group of (216 F-43m, 186 P-63mc, 186 P-63mc), respectively. Through our assessments, we determined that (8×8×8) BZ k-point cell densities and planar wave discontinuities of 750 eV for ZnTe, 850 eV for ZnS, and 800 eV for ZnO were adequate. In general, the

[†] ***Cite as:*** F. Benlakhdar, I. Bouchama, T. Chihi, I. Ghebouli, M.A. Ghebouli, Z. Zerrougui, K. Khatir, M.A. Saeed, East Eur. J. Phys. 3, 413 (2023), https://doi.org/10.26565/2312-4334-2023-3-45
© F. Benlakhdar, I. Bouchama, T. Chihi, I. Ghebouli, M.A. Ghebouli, Z. Zerrougui, K. Khatir, M.A. Saeed, 2023

GGA approach is preferred over LDA because LDA tends to underestimate the lattice parameters and cell volume, whereas GGA overestimates them. To approximate the GGA method, we used the Perdew-Burke-Ernzerhof [12] approach to estimate the band gap. We conducted geometric optimization with a precision of $1 \times 10^{-5}$ eV/atom and we used the Broyden–Fletcher–Goldfarb–Shanno (BFGS) algorithm to relax at the lowest energy levels, with force, pressure, and displacement values set at 0.001 eV/A, 0.05 GPa, and $5.0\times 10^{-4}$ Å, respectively. We examined the electronic structures and other optical properties using total and partial densities of states, such as TDOS and PDOS, to achieve a more refined geometry.

## III. RESULTS AND DISCUSSIONS

### a. Structural Properties

In the first stage of our study, we performed calculations to determine the equilibrium structural parameters of ZnX (X = Te, S, and O), including the lattice constant a0, size modulus B0, and its first derivative B0'. The crystal structure of ZnX (X = Te, S, and O) is shown in Fig. 1. We focused on investigating the structural properties of ZnX and optimizing the lattice constants, and the results are presented in Table 1. The accuracy and validity of our research are confirmed by comparing our findings with existing theoretical and experimental data (as shown in Table 1). Our calculations show that the lattice constant a0 is 6.28 Å for ZnTe, 5.62 Å for ZnS, and 3.25 Å for ZnO. These values are slightly larger than the experimentally recorded values of 6.1 Å [13], 5.41 Å [13], and a = 3.249 Å, c = 5.204 Å [9], respectively. However, this discrepancy can be attributed to the difference in the atomic radii of ZnTe, ZnS, and ZnO, as well as the larger total energies, lattice relaxation constants, volume coefficients, and ground state energy of each material.

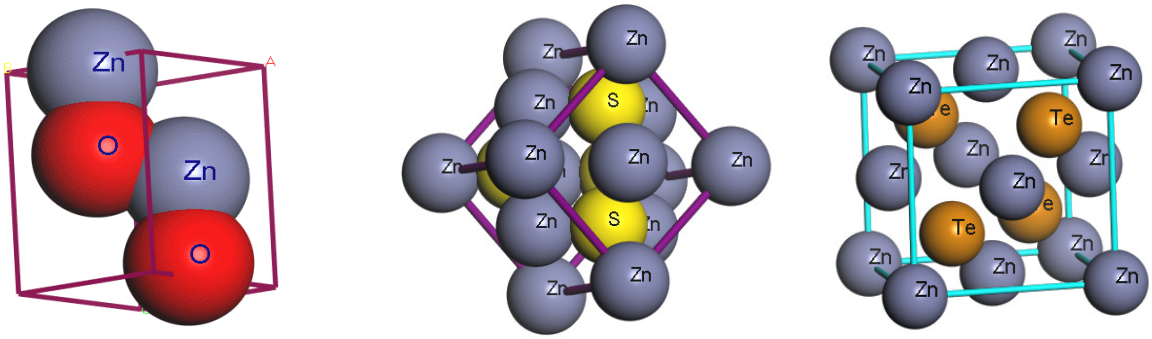


**Figure 1.** Crystal structures of: (a) ZnTe, (b) ZnS and (c) ZnO compounds.

We have optimized the structures of ZnTe, ZnS and ZnO at different pressure by fitting the Murnaghan equation of state [14], which gives the variation of the total energy as a function of the volume and given by:

$$E(V) = E_0 + \left[\frac{B_0 V}{B'(B'-1)}\right].\left[B'\left(1-\frac{V_0}{V}\right) + \left(\frac{V_0}{V}\right)^{B'} - 1\right] \quad (1)$$

where $V_0$, $B$ and $B'$ are the volume at equilibrium, the bulk modulus and its derivative. The modulus of compressibility and its pressure derivative $B_0$' written as follows:

$$B0' = \frac{\partial B}{\partial P} \quad (2)$$

The fits of our data regarding the relative lattice constant $a_0$ (Å), bulk modulus $B_0$ (GPa) and the volume are given in Table 1.

**Table 1.** Calculated lattice constant $a_0$ (Å), bulk modulus $B`_0$ (GPa) for ZnX (X = Te, S and O) compound compared with already published data.

| *Compound* | *$a_0$(Å)* | *V(Å$^3$)* | *$B_0$(GPa)* | *B'$_0$* |
|---|---|---|---|---|
| | *6.28[n]* | *61.986[n]* | *41.30[n]* | *4.266[n]* |
| | *6.187[d]* | *52.66[b]* | *49.70[b]* | *4.45[b]* |
| | *6.103[i]* | *52.96[c]* | *51.40[c]* | *4.50[c]* |
| *ZnTe* | *6.16[e]* | *56.73[j]* | *55.21[h]* | *4.60[h]* |
| | *6.00[h]* | *58.73[b]* | *45.20[j]* | *4.63[j]* |
| | *6.17[b]* | *56.82[b] Exp.* | *45.25[b]* | *4.26[b]* |
| | *6.1[e] Exp* | | *50.9[h] Exp.* | *5.04[h] Exp.* |
| | *5.62[n]* | *44.60[n]* | *62.043[n]* | *4.094[n]* |
| | *5.451[d]* | | *75.6[e]* | *4.44[h]* |
| *ZnS* | *5.44[e]* | | *89.67[h]* | *4.00[h] Exp.* |
| | *5.342[h]* | | *75[h] Exp.* | |
| | *5.41[e] Exp* | | | |

| *Compound* | *$a_0$(Å)* | *V(Å$^3$)* | *$B_0$(GPa)* | *B'$_0$* |
|---|---|---|---|---|
| *ZnO* | *3.250*[n] | *55.126*[n] | *115.923*[n] | *4.486*[n] |
| | *a = 3.244*[d] | *45.82*[d] | *159.5*[g] | *4.5*[g] |
| | *c = 5.027*[d] | *47.719*[f] | *128.72*[i] | *4.38*[i] |
| | *a = 3.249*[f] | *49.461*[k] | *183*[g] *Exp.* | *4*[g] *Exp.* |
| | *c = 5.216*[f] | *48.335*[k] *Exp.* | | |
| | *a = 3.198*[g] | | | |
| | *c = 5.167*[g] | | | |
| | *a = 3.2496*[g] *Exp.* | | | |
| | *c = 5.2042*[g] *Exp.* | | | |

[a]Ref [15], [b]Ref [16], [c]Ref [17], [d]Ref [1], [e] Ref [13], [f]Ref [18], [g]Ref [9], [h]Ref [3], [i]Ref [19], [j]Ref [17], [k] Ref [20], [l] Ref [2]
[n] Present calculations.

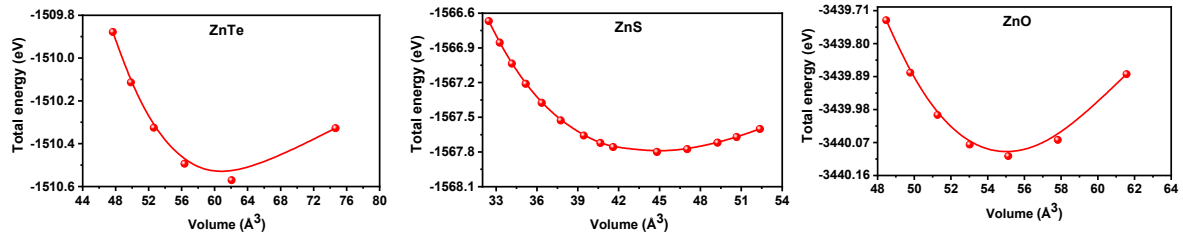


**Figure 2.** Total energy versus volume for ZnX (X = Te, S and O) compounds.

### b. Electronic properties

The band structure and the total density of states (TDOS) and partial density of states (PDOS) calculated with optimized values were utilized to examine the electronic properties of ZnX (X = Te, S and O). The band-gap energy, particularly, provided insights into the bonding nature. The PBE-GGA approximation was used in the calculations. The computed band-gap of the three compounds revealed that all were semiconducting in nature, as illustrated in Fig. 3. In addition, the direct band-gap values for ZnX (X = Te, S and O) were 2.436, 2.698, and 1.721 eV, respectively. The conduction and valence bands were situated above and below the Fermi level. Both the bottom of the conduction band and the top of the valence band were located at the same point k (G - G), confirming that ZnX (X = Te, S and O) is a direct band-gap. All the calculated band-gap values for ZnX (X = Te, S and O) at 0 GPa are presented in Table 2. All values shown in Table 2 are consistent with theoretical and experimental data reported in other references that employ the PBE-GGA approximation. It is worth noting that the calculated band-gaps were lower than experimental values, which is attributed to the known Kohn-Sham DFT calculation error. The relatively higher band-gap energy of ZnTe, ZnS and ZnO compounds suggests that these compounds could potentially exhibit enhanced optical properties.

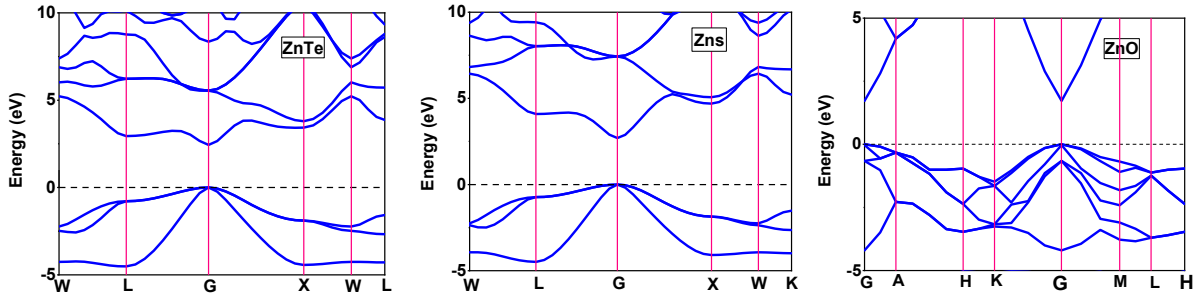


**Figure 3.** Calculated band structure of ZnX (X = Te, S and O) compounds using PBE-GGA approximation.

**Table 2.** Calculated band-gap value of ZnX at 0 GPa.

| *Compound* | *This work* | *Other theoretical calculations* | *Experiments* |
|---|---|---|---|
| *ZnTe* | *2.436*[n] | *1.711*[d]<br>*1.804*[f] | *2.39*[f] |
| *ZnS* | *2.698*[n] | 2.07[e]<br>*2.11*[g]<br>*1.317*[h]<br>*2.17*[j] | *3.68*[h] |
| *ZnO* | *1.721*[n] | *0.8*[a]<br>*3.38*[c]<br>*0.73*[k]<br>*3.37*[l] | |

[a] Ref [21], [c] Ref [18], [d] Ref [22], [e] Ref [23], [j] Ref [24], [k] Ref [25], [g] Ref [26], [h] Ref [27], [l] Ref [28], [n] Present calculations.

### c. Density of States

To better understand the band and optical properties of ZnX (X = Te, S and O), it is important to investigate the electronic density of states (DOS) [29] and its relationship with the band structure. In this study, the DOS was determined and its connection with the band structure was examined. The chemical bonding of ZnX was illustrated by counting single atoms using partial DOS (PDOS) and all atoms using total DOS (TDOS). The electronic DOS is a crucial electronic property as it provides a deeper understanding of the band structure. Fig. 4 shows the TDOS and PDOS obtained using the GGA-PBE approximation, with the Fermi level taken as the energy origin. The electron configuration of Zn, Te, S, and O were 3d24s2, 3s23p6, 4s24p65s2, and 2s22p4, respectively. There are two regions, BV and BC, on both sides of the Fermi level: the BV region, dominated by Te-p, S-p, and O-p states, is centered between -5 eV and 0 eV for all three compounds. The second region, BC, centered between 0 eV and 5 eV, is dominated by Zn-s-p, Te-s-p, and S-s-p states. These results are consistent with previous reports.

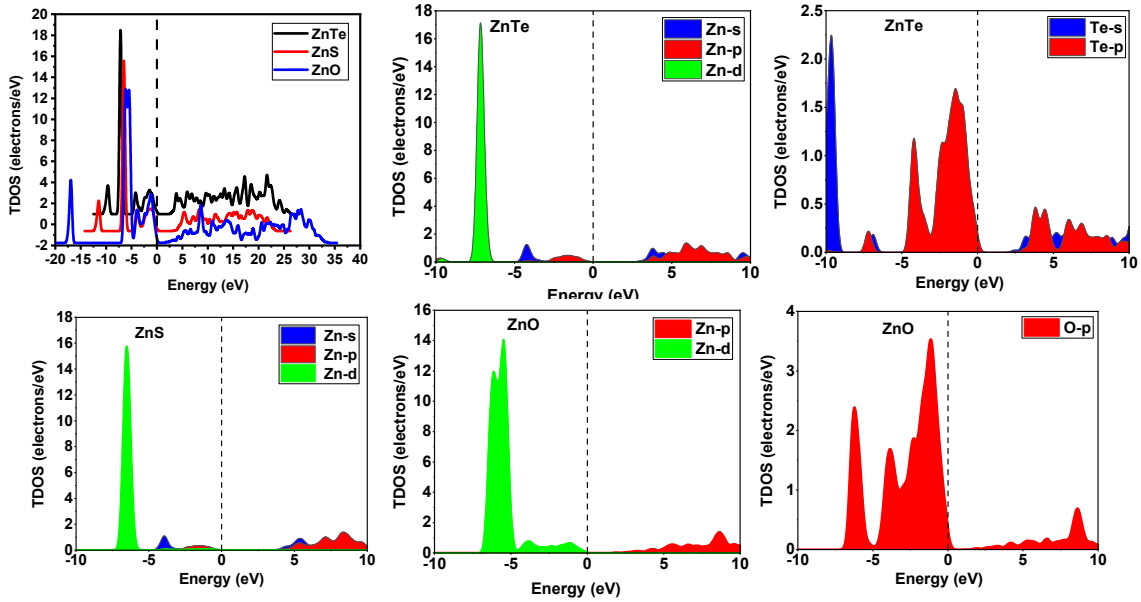


**Figure 4.** TDOS and PDOS spectra calculated using GGA-PBE approximation of ZnX (X = Te, S and O) compounds.

### d. Optical Properties

The investigation of photonic properties is crucial for the studied compounds, as they have potential applications in photovoltaic devices and the semiconductor industry. To describe the optical properties of these materials, the transverse dielectric function ε(ω) [30] is used. The frequency-dependent dielectric constants have been calculated using the following formula:

$$\varepsilon(\omega) = \varepsilon_1(\omega) + i.\varepsilon_2(\omega) \tag{3}$$

The dielectric function is characterized by the real and imaginary parts, ε1(ω) and ε2(ω), respectively [31]. The real part of ε1(ω) corresponds to the dispersion of incident photons by the material, while the imaginary part of ε2(ω) represents the energy absorbed by the material. The complex dielectric function ε(ω) is made up of two contributions: intraband and interband transitions [31]. The contribution from intraband transitions is significant only for metals. The interband transitions can be further divided into direct and indirect transitions. In this study, the indirect interband transitions, which involve phonon scattering and contribute minimally to ε(ω), were neglected.

The complex dielectric function components were utilized to determine other optical parameters, including reflectivity R, refractive index n, optical conductivity σ, and absorption α [32]. The equations used to calculate these parameters are as follows:

$$R(w) = \frac{(n-1)^2 + k^2}{(n+1)^2 + k^2} \tag{4}$$

$$n(w) = \frac{\sqrt{\varepsilon_1{}^2(w) + \varepsilon_2{}^2(w)} + \varepsilon_1{}^2}{\sqrt{2}} \tag{5}$$

$$Re[\sigma(w)] = \frac{w}{4\pi}\varepsilon_2(w) \tag{6}$$

$$\alpha(w) = \sqrt{2}(w)\left[\sqrt{\varepsilon_1{}^2(w) + \varepsilon_2{}^2(w)} - \varepsilon_1(w)\right]^{\frac{1}{2}} \tag{7}$$

Fig. 5 through 9 depict various optical properties of ZnX (X = Te, S and O), including reflection spectra, absorption spectra, imaginary and real parts of the dielectric function, and photoconductivity.

### 1. Reflectivity R

The reflectivity R of a compound ZnX (where X = Te, S, or O) can be accurately predicted using computational tools such as the CASTEP program. For example, CASTEP simulations have shown that ZnTe exhibits a high reflectivity of approximately 96% in the infrared region, which makes it a promising material for infrared detectors and solar cells. Similarly, ZnS and ZnO have been found to exhibit high reflectivity in the visible and ultraviolet regions, respectively, with values reaching up to 87% and 96%. By tuning the composition and morphology of ZnX compounds, researchers can manipulate their reflectivity to suit specific applications. For instance, by growing ZnO thin films with a specific orientation, researchers can achieve high reflectivity of visible light while maintaining transparency.

Our analysis, as presented in Fig. 5, reveals that the reflectivity peaks of ZnTe, ZnS, and ZnO compounds increase at low energy (up to 7 eV), and decrease significantly at high energy (below 20 eV), as the forbidden bandwidth reduces.

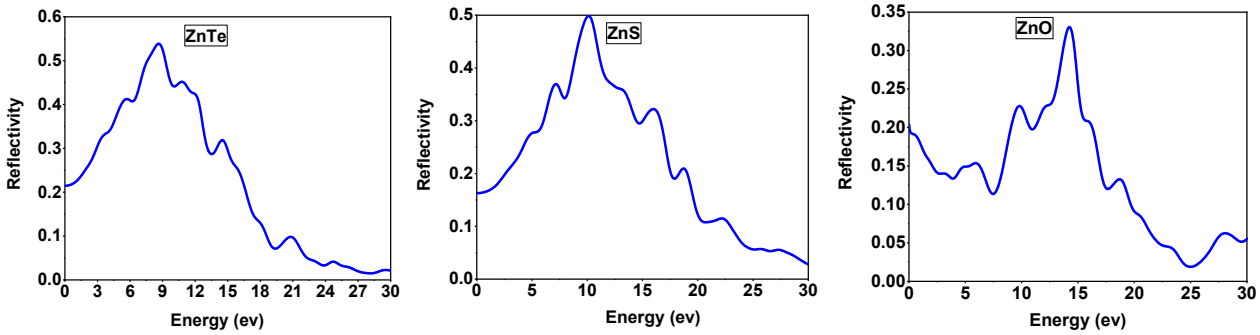


**Figure 5.** Reflectivity R as a function of energy of ZnTe, ZnS and ZnO compounds calculated using GGA-PBE approximation.

### 2. Absorption A

The absorption, denoted by A, is an important optical property of materials that describes the amount of light absorbed by the material. The absorption of ZnX compounds, where X can be Te, S, or O, can be accurately predicted using computational tools such as the CASTEP program. The results have shown that ZnTe has a high absorption coefficient of approximately 25 × $10^4$ $cm^{-1}$ in the mid-infrared region, making it a promising material for mid-infrared detectors and emitters. Similarly, ZnS and ZnO have been found to exhibit high absorption in the ultraviolet and visible regions, respectively, with values reaching up to 3 × $10^5$ $cm^{-1}$. By understanding the absorption properties of ZnX compounds, researchers can design materials with specific absorption properties for various optoelectronic applications.

According to our study, when more electrons can be easily excited from the valence band to the conduction band, less energy is required, resulting in a redshift at the absorption edge. In this scenario, the probability of valence band electron guide transitioning to the excited state increases, leading to an obvious increase in the number of absorption peaks. Our findings, presented in Fig. 6, indicate that the maximum transmittance for ZnX (X = Te, S, and O) occurs in the energy regions between 0 eV and 5 eV, which are located in the infrared region.

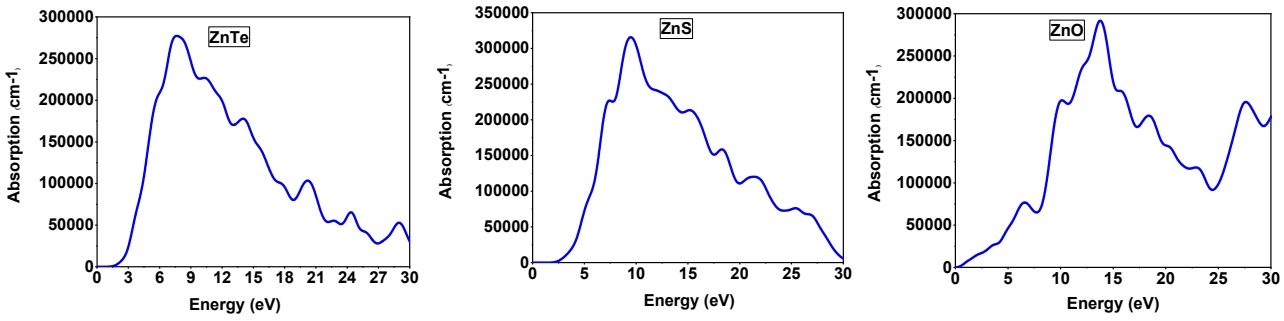


**Figure 6.** Absorption A as a function of energy of ZnTe, ZnS and ZnO compounds calculated using GGA-PBE approximation

### 3. Refractive index

The refractive index, denoted by n, is an important optical property that characterizes how light propagates through a material. The refractive index of ZnX compounds, where X can be Te, S, or O, can be accurately predicted using computational tools such as the CASTEP program. We have shown that the refractive index of ZnTe is approximately 2.5 in the mid-infrared region, making it a promising material for applications such as infrared lenses and waveguides. Similarly, ZnS and ZnO have been found to exhibit high refractive indices in the ultraviolet and visible regions, respectively, with values reaching up to 2 and 1.9. By understanding the refractive index of ZnX compounds, researchers can design materials with specific optical properties for various optoelectronic applications.

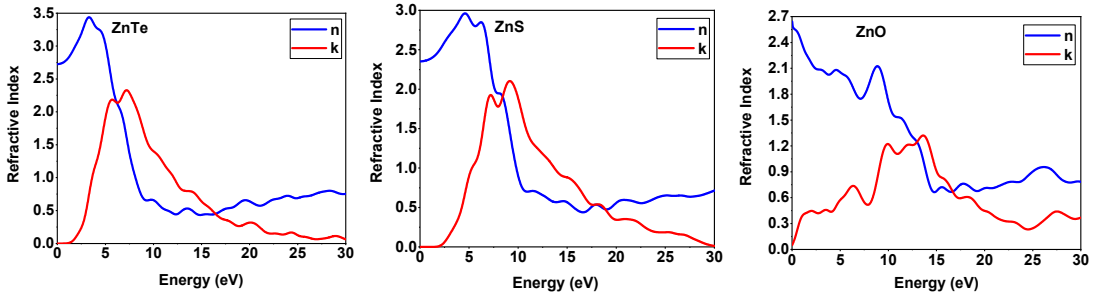


**Figure 7.** Refractive index as a function of energy of ZnTe, ZnS and ZnO compounds calculated using GGA-PBE approximation.

## 4. Dielectric function

The dielectric function, denoted by ε, is an important optical property that characterizes the response of a material to an external electric field. The simulation results using CASTEP have shown that the dielectric function of ZnTe is approximately 12 in the mid-infrared region, making it a promising material for applications such as infrared detectors and emitters. Similarly, ZnS and ZnO have been found to exhibit high dielectric functions in the ultraviolet and visible regions, respectively, with values reaching up to 9 and 5. By understanding the dielectric function of ZnX compounds, researchers can design materials with specific optical properties for various optoelectronic applications.

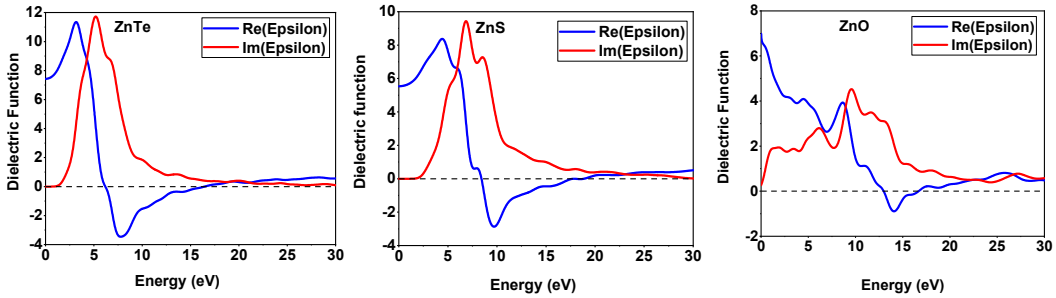


**Figure 8.** Dielectric function as a function of energy of ZnTe, ZnS and ZnO compounds calculated using GGA-PBE approximation.

## 5. Conductivity

The conductivity, denoted by σ, is an important electronic property that characterizes the ability of a material to conduct electric current. The conductivity of ZnX can be accurately predicted using computational tools such as the CASTEP program. The simulation results have shown that ZnTe has a high electrical conductivity of approximately 7 S/m at room temperature, making it a promising material for applications such as solar cells and thermoelectric devices. ZnS and ZnO materials exhibit moderate to high electrical conductivity, respectively, with values reaching up to 9 and 5 S/m.

Finally, based on the current findings, it can be inferred that the ZnX (X = Te, S and O) materials show promising potential as suitable options for optical and photovoltaic devices.

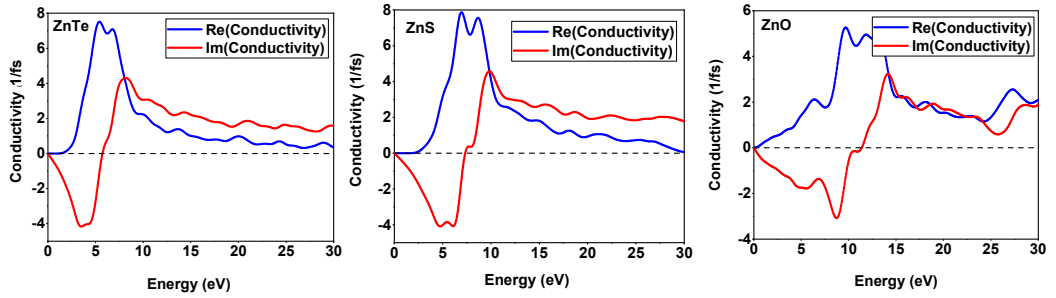


**Figure 9.** Conductivity as a function of energy of ZnTe, ZnS and ZnO compounds calculated using GGA-PBE approximation.

## IV. Application to the substrate Cu(In,Ga)Se$_2$ solar cells

The conventional method of fabricating Cu(In,Ga)Se$_2$ (CIGS) thin-film solar cells involves the use of a substrate configuration that incorporates a CdS buffer layer and a doped ZnO or ITO window layer. This configuration has demonstrated conversion efficiencies exceeding 22% [29]. The exceptional optoelectronic properties of ZnX (X = Te, Se, S …etc) buffer layers have led to increased attention as a potential alternative to CdS buffer layers in recent years [33]. It is widely believed that the buffer layers play a critical role in preventing shunting through the TCO/CIGS interface, and they should possess suitable properties that help to minimize carrier recombination at the buffer/CIGS interface [34]. For

example, the efficiency of CIGS solar cells decreases significantly due to severe shunting when a conventional ZnO/TCO is directly deposited onto the CIGS layer [35]. According to some studies, the buffer layer demonstrated a higher level of electrical resistance compared to the top contact layer, which is highly conductive [30]. In this study, the use of ZnTe and ZnS as buffer layers in the substrate CIGS solar cell, along with the incorporation of the ZnO layer as a window layer, were investigated.

### IV.1. Device settings and simulation process

Fig. 10 shows schematic of the substrate n++-ZnO/n-ZnS/p-Cu(In,Ga)$Se_2$ and n++-ZnO/n-ZnTe/p-Cu(In,Ga)$Se_2$ solar cell hetero-structures. To study the transport physics of these structures, the SCAPS-1D software solution solves the dipolar issues of the device using the Poisson equation and continuity equations for both electrons and holes. The SCAPS-1D simulator provides a software environment that can accurately replicate the behavior of a real solar cell [32,36]. Typically, the simulation process for a solar cell would require following the steps outlined in Fig. 11 through a series of screen-shots. The initial screenshot, labeled (a), displays the standard information input panel of the SCAPS-1D graphical user interface. This panel provides access to input buttons that enable the user to specify the simulation model and view the device's operating conditions, structure, and material parameters. The device simulation utilizes DOS mode. One particular layer's structure and material parameters, along with optical properties and defects, are displayed in screenshot (b). The results of light J-V characteristics in the form of a curve and axes are shown in screenshot (c). The simulation uses AM1.5 illumination spectrum with an incident power of 100 mW/cm$^2$. Table 3 summarizes the input parameters of each layer, including thickness, permittivity constant, band gap, electron affinity, electron/hole mobility, effective density of states in conduction/valence band, donor/acceptor concentration, defect concentration, and absorption coefficient within a range of 320 - 1100 nm wavelength. The thermal velocity recombination for holes/electrons at front and back contacts is $1.0 \times 10^7$ cm/s.

All data that have been previously calculated using CASTEP are being considered in the simulation.

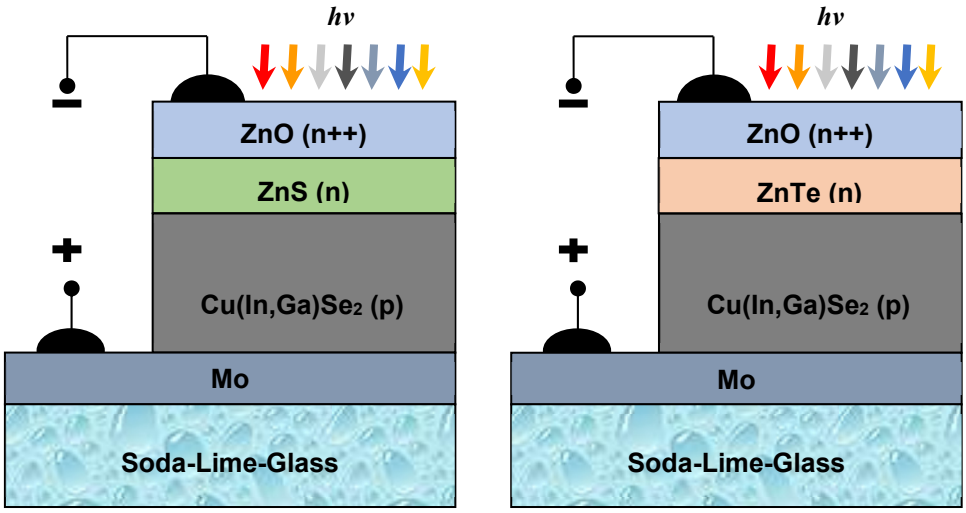


**Figure 10.** Schematic of the n++-ZnO/n-ZnS/Cu(In,Ga)$Se_2$ and n++-ZnO/n-ZnS/Cu(In,Ga)$Se_2$ solar cell structures

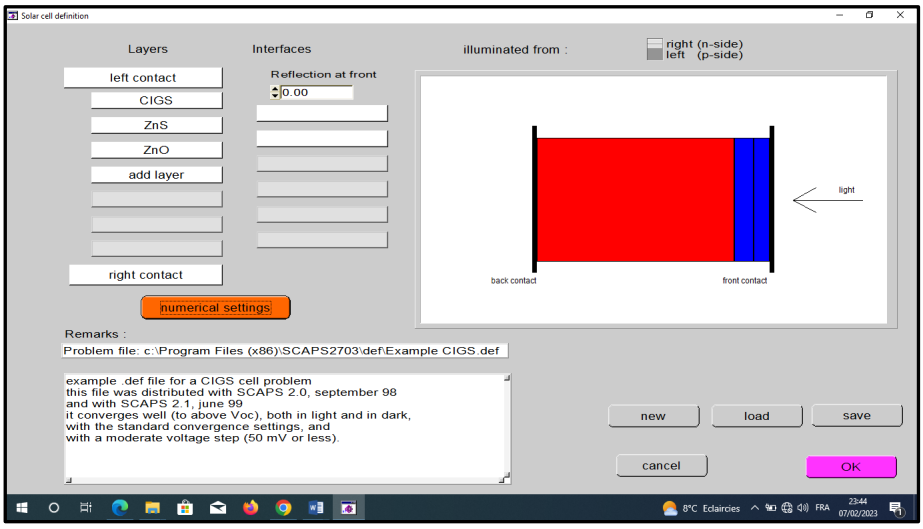


(a)

**Figure 11.** Typical data input panels of the SCAPS-1D graphical user interface, allowing to configure the solar cell device and its corresponding settings (*continued on the next page*)

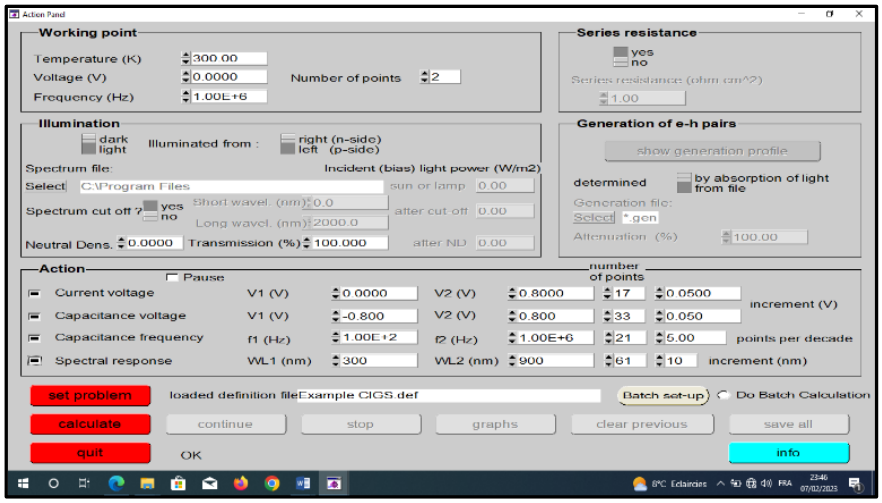


(b)

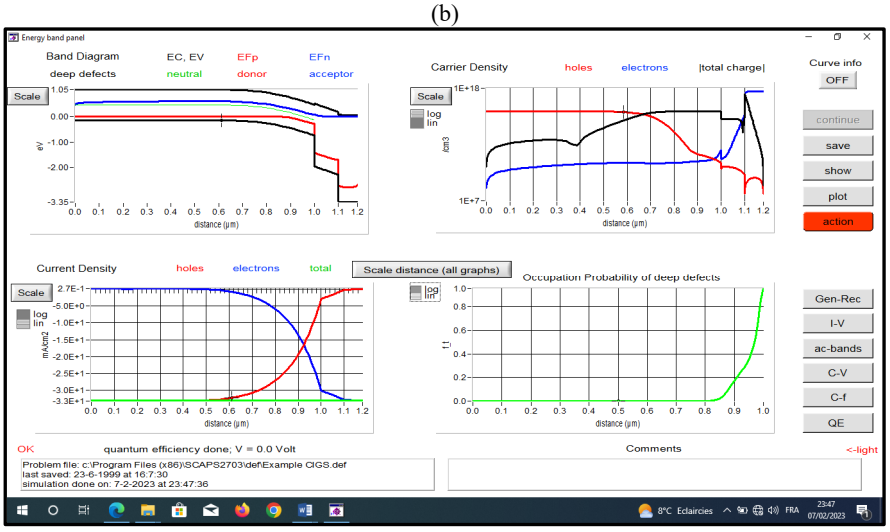


(c)

**Figure 11.** Typical data input panels of the SCAPS-1D graphical user interface, allowing to configure the solar cell device and its corresponding settings (*continued*)

**Table 3.** Settings for ZnO, ZnTe, ZnS and Cu(In,Ga)$Se_2$ layers used in the simulation.

| *Parameters* | *Cu(In,Ga)$Se_2$ Absorber* | *ZnTe buffer* | *ZnS buffer* | *ZnO window* |
|---|---|---|---|---|
| *Thickness (nm)* | *3000* | *100* | *100* | *200* |
| *Band gap $E_g$ (eV)* | *1.12* | *2.43* | *2.69* | *3.3* |
| *Electron affinity $\chi_e$ (eV)* | *4.1* | *4.07* | *4.09* | *4.09* |
| *Relative permittivity $\varepsilon_r$ (-)* | *13.6* | *10* | *10* | *9* |
| *Electron mobility $\mu_n$ ($cm^2/V\,s$)* | *100* | *100* | *100* | *100* |
| *Electron mobility $\mu_p$ ($cm^2/V\,s$)* | *25* | *25* | *25* | *25* |
| *Conduction band effective density of states $N_C$ ($cm^{-3}$)* | *$2.0\times10^{o}$* | *$2.0\times10^{o}$* | *$2.0\times10^{o}$* | *$4.0\times10^{o}$* |
| *Conduction band effective density of states $N_V$ ($cm^{-3}$)* | *$2.0\times10^{o}$* | *$1.5\times10^{p}$* | *$1.5\times10^{p}$* | *$9.0\times10^{o}$* |
| *shallow donor density ($1/cm^3$)* | *0* | *$1.0\times10^{q}$* | *$1.0\times10^{q}$* | *$1.0\times10^{p}$* |
| *shallow acceptor density ($1/cm^3$)* | *$5.5\times10^{r}$* | *0* | *0* | *0* |

[o] Ref [37], [p] Ref [31], [q] Ref [38], [r] Ref [39].

### IV.2. Effect of CIGS absorber thickness on solar cell performance

In an attempt to determine the most favorable thickness for a high-performance substrate CIGS solar cell that employs ZnTe and ZnS buffer layers, the thickness of the CIGS absorber was modified.

#### 1. Case of ZnO/n-ZnS/p-CIGS/Mo solar cell structure

It is desirable to reduce the thickness of the absorber layer, *d*(CIGS), in order to lower costs while still maintaining high performance. ZnTe and ZnS buffer layers can help achieve this goal due to the abundance of these materials. In the

calculations, the thickness of the buffer layers is fixed at 100 nm. As shown in Fig. 12, the short-circuit current density (*J*sc), open circuit voltage (*V*oc), Fill Factor (*FF*), and power conversion efficiency (η) are all affected by the thickness of the CIGS absorber layer. For absorber thicknesses up to 4 µm, *J*sc remains around 32.1 mA/cm$^2$ and *V*oc is above 0.61 Volt. However, for the thinnest CIGS absorber layer, there is a slight reduction in *V*oc which may be due to an increased influence of recombination at the Mo back contact layer, resulting in a smaller effective minority carrier lifetime. The fill factor slightly increases but remains above 79% for all absorber thicknesses greater than 4 µm. The short-circuit current density and open circuit voltage show a strong dependence on the absorber thickness, *J*sc increases from 29.12 mA/cm$^2$ to 32.08 mA/cm$^2$ as the CIGS absorber thickness varies from 1 to 4 µm. For devices thinner than 1 µm, current loss may be due to optical and/or electrical losses. The losses in *J*sc and *V*oc mainly contribute to the conversion efficiency losses. The optimum thickness for the CIGS absorber layer is greater than 4 µm, which results in a maximum conversion efficiency of 15.6% with *FF* = 78.5%, *V*oc = 0.61 Volt and *J*sc = 32.1 mA/cm$^2$.

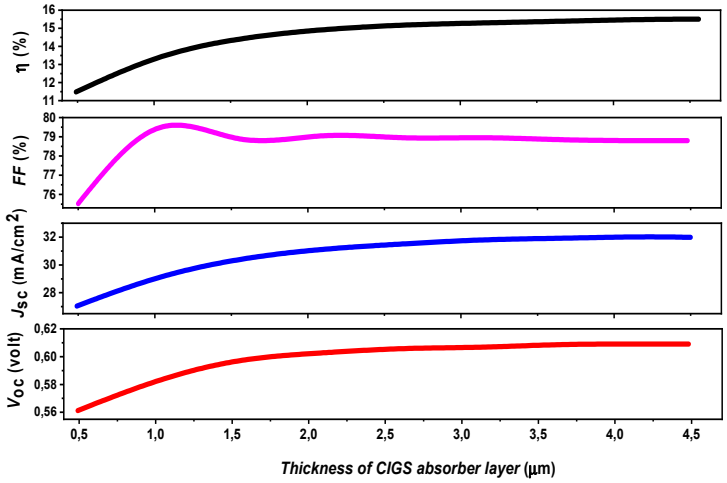


**Figure 12.** Solar cell performance using ZnS buffer layer as a function of the p-CIGS thickness.

### 2. Case of ZnO/n-ZnTe/p-CIGS/Mo solar cell structure

Fig. 13 presents the performance of ZnO/ZnTe/CIGS/Mo solar cell as a function of CIGS absorber thickness. It shows that the recorded efficiency is 14.66% and 16.58% at the CIGS thickness of 1 µm and 4 µm, respectively.

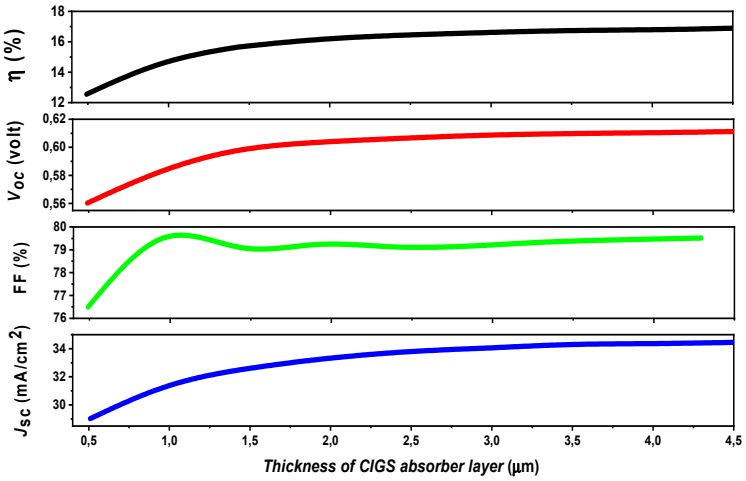


**Figure 13.** Solar cell performance using ZnTe buffer layer as a function of p-CIGS thickness.

A comparison of these results with the 16.12% efficiency at 2 µm reveals that decreasing the absorber thickness by 1 µm leads to an 11.58% drop in efficiency, whereas increasing it by 1 µm results in only a 3.8% increase in efficiency. This trend continues to hold for absorber thicknesses more than 2 µm. These findings support the theoretical assumption that a thickness of around 2 µm is sufficient to absorb most of the incident light. However, reducing the absorber layer thickness below this value would bring the back contact too close to the depletion region, which would facilitate electron capture by the back contact during the recombination process. The open circuit voltage (*V*oc) and short circuit current density (*J*sc) increase with the thickness of the absorber layer, primarily due to the longer wavelengths' absorption, which contributes to electron-hole pair generation. When *d*(CIGS) is greater than 4 µm, the maximum Fill Factor of 79.5% is obtained. The highest efficiency of approximately 16.58%, with *FF* = 79.5%, *V*oc = 0.61 Volt, and *J*sc = 34.05 mA/cm$^2$ can be achieved when *d*(CIGS) is approximately 4 µm.

## III. CONCLUSIONS

The use of computational tools like CASTEP provides a powerful tool for the design and optimization of such materials, enabling the development of advanced optoelectronic devices. In this paper, the electronic structure and optical properties of ZnX systems were studied using the first principles of the ultra-smooth pseudovoltage method of density functional theory and the generalized gradient approximation method using the CASTEP tool. The search showed the following results: The network parameters took different values; Therefore, it is possible to deposit them on different substrates. The binary alloy is interesting, because it has a wide bandgap (2.436 eV, 2.698 eV, 1.721 eV) for ZnTe, ZnS and Zn0, respectively. From the results obtained, the structural, physical and optical properties are in close agreement with the available theoretical and experimental data which indicate the accuracy of the proposed calculation scheme. The properties of pure ZnX (X = Te, S, O) materials indicate that these materials have great potential for use in solar cells. The outcomes of the calculation reveal that although the efficiency grew alongside the absorber thickness, *d*(CIGS), the pace of this increase was much less beyond 2 μm. The result concludes that the CIGS absorber layer's ideal thickness is likely to exceed 4 μm.

### ORCID

**Faiza Benlakhdar**, https://orcid.org/0009-0003-1131-6289

### Acknowledgments

The authors show recognition to the scientists, at the Department of Electronics and Information Systems (ELIS) of the University of Gent, Belgium, that developed the freely SCAPS-1D simulator.

### REFERENCES

[1] B.G. Svensson, “Electronic structure and optical properties of Zn X ( X =O, S, Se, Te),” pp. 1–14, 2018.
[2] M. Lee, Y. Peng, and H. Wu, “Effects of intrinsic defects on electronic structure and optical properties of Ga-doped ZnO,” J. Alloys Compd. **616**, 122-127 (2014)ю https://doi.org/10.1016/j.jallcom.2014.07.098
[3] R. Khenata, “Elastic, electronic and optical properties of ZnS, ZnSe and ZnTe under pressure,” Computational Materials Science, **38**, 29-38 (2006). https://doi.org/10.1016/j.commatsci.2006.01.013
[4] Y. Yu, J. Zhou, H. Han, and C. Zhang, “Ab initio study of structural , dielectric , and dynamical properties of zinc-blende ZnX (X = O, S, Se, Te),” Journal of Alloys and Compounds, **471**, 492-497 (2009). https://doi.org/10.1016/j.jallcom.2008.04.039
[5] S. Jeetendra, H. Nagabhushana, K. Mrudula, C.S. Naveen, P. Raghu, and H.M. Mahesh, “Concentration Dependent Optical and Structural Properties of Mo doped ZnTe Thin Films Prepared by e-beam Evaporation Method,” Int. J. Electrochem. Sci. **9**, 2944-2954 (2014). http://www.electrochemsci.org/papers/vol9/90602944.pdf
[6] S.M. Ali, A.A.A. Shehab, and S.A. Maki, “Study of the Influence of Annealing Temperature on the Structural and Optical Properties of ZnTe Prepared by Vacuum Thermal Evaporation Technique,” Ibn Al-Haitham Journal for Pure and Applied sciences, **31**(1), 50-57 (2018). https://doi.org/10.30526/31.1.1851
[7] Y. Yu et al., “Ab initio study of structural, dielectric, and dynamical properties of zinc-blende ZnX (X= O, S, Se, Te),” Journal of alloys and compounds, 471(1-2), 492-497 (2009). https://doi.org/10.1016/j.jallcom.2008.04.039
[8] D. Bahri and L. Amirouche, “Ab initio study of the structural , electronic and optical properties of ZnTe compound,” AIP Conference Proceedings, **1653**(1), (2015). https://doi.org/10.1063/1.4914210
[9] J. Serrano, Y. Tech, A. H. Romero, and R. Lauck, “Pressure dependence of the lattice dynamics of ZnO : An ab initio approach,” Physical Review B, **69**, 094306 (2004). https://doi.org/10.1103/PhysRevB.69.094306.
[10] V.O.I. Ume, P. Walter, L. Cohen, and Y. Petroff, “Calculated and Measured Reflectivity of ZnTe and ZnSef,” Phys. Rev. B, **1**, 2661 (1970). https://doi.org/10.1103/PhysRevB.1.2661
[11] M. Caid *et al.*, “Electronic structure of short-period ZnSe/ZnTe superlattices based on DFT calculations,” Condensed Matter Physics, **25**(1), 1-10 (2022). https://doi.org/10.5488/CMP.25.13701
[12] F. Parandin, J. Jalilian, and J. Jalilian, “Tuning of electronic and optical properties in ZnX ( X = O, S, Se and Te ) monolayer : Hybrid functional calculations,” Chemical Review & Letters, **2**(2), 76-83 (2019). https://doi.org/10.22034/crl.2019.195774.1019
[13] Z. Nourbakhsh, “Structural , electronic and optical properties of ZnX and CdX compounds (X = Se , Te and S) under hydrostatic pressure,” J. Alloys Compd. **505**(2), 698-711 (2010). https://doi.org/10.1016/j.jallcom.2010.06.120.
[14] F.D. Murnaghan, “The Compressibility of Media under Extreme Pressures,” Proceedings of the National Academy of Sciences of the United States of America, **30**(9), 244-247 (1944). https://www.jstor.org/stable/87468
[15] M. Safari, Z. Izadi, J. Jalilian, and I. Ahmad, “Metal mono-chalcogenides ZnX and CdX (X = S , Se and Te) monolayers : Chemical bond and optical interband transitions by first principles calculations,” Phys. Lett. A, **381**(6), 663-670 (2017). https://doi.org/10.1016/j.physleta.2016.11.040.
[16] S. K. Gupta, S. Kumar, and S. Auluck, “Structural, electronic and optical properties of high pressure stable phases of ZnTe,” Physica B: Condensed Matter, **404**, 3789-3794 (2009). https://doi.org/10.1016/j.physb.2009.06.149
[17] A.A. Audu, W.A. Yahya, and A.A. Abdulkareem, Physics Memoir: Journal of Theoretical & Applied Physics, “Ab initio Studies of the Structural, Electronic and Mechanical Properties of $Zn_{1-x}Cr_x$ e,” **3**, 38-47 (2021).
[18] M. Achehboune, M. Khenfouch, I. Boukhoubza, I. Derkaoui, B.M. Mothudi, I. Zorkani, A. Jorio, “Effect of Yb Concentration on the Structural, Magnetic and Optoelectronic Properties of Yb Doped ZnO : First Principles Calculation”. http://dx.doi.org/10.21203/rs.3.rs-877060/v1
[19] R. John, and S. Padmavathi, “Ab Initio Calculations on Structural, Electronic and Optical Properties of ZnO in Wurtzite Phase,” Cryst. Struct. Theory Appl. **5**(2), 24-41 (2016). https://doi.org/10.4236/csta.2016.52003
[20] R. Chowdhury, S. Adhikari, and P. Rees, “Optical properties of silicon doped ZnO,” Phys. B Condens. Matter, **405**(23), 4763-4767 (2010). https://doi.org/10.1016/j.physb.2010.08.072

[21] C. Feng *et al.*, "First-principle calculation of the electronic structures and optical properties of the metallic and nonmetallic elements-doped ZnO on the basis of photocatalysis," Phys. B Condens. Matter, **555**, 53-60 (2019). https://doi.org/10.1016/j.physb.2018.11.043.
[22] L. Chen, X. Zhou, and J. Yu, "First-principles study on the electronic and optical properties of the ZnTe/InP heterojunction," *J.* Comput. Electron. **18**(3), 749-757 (2019). https://doi.org/10.1007/s10825-019-01358-8
[23] A.M. Ghaleb, and A.Q. Ahmed, "Structural, electronic, and optical properties of sphalerite ZnS compounds calculated using density functional theory (DFT)," Chalcogenide Lett. **19**(5), 309-318 (2022). https://doi.org/10.15251/CL.2022.195.309
[24] Q. Hou, and S. Sha, "Effect of biaxial strain on the p-type of conductive properties of (S, Se, Te) and 2 N co-doped ZnO," Mater. Today Commun. **24**, 101063 (2020). https://doi.org/10.1016/j.mtcomm.2020.101063
[25] Md.A. Momin, Md.A. Islam, A. Majumdar, "Influence on structural , electronic and optical properties of Fe doped ZnS quantum dot : A density functional theory based study," Quantum Chemistry, **121**(1), 1-13 (2020). https://doi.org/10.1002/qua.26786
[26] M. Dong, P. Zhou, C. Jiang, B. Cheng, and J. Yu, "First-principles investigation of Cu-doped ZnS with enhanced photocatalytic hydrogen production activity State Key Laboratory of Advanced Technology for Materials Synthesis and," Chem. Phys. Lett. **668**, 1-6 (2016). https://doi.org/10.1016/j.cplett.2016.12.008
[27] A. Pattnaik, M. Tomar, P.K. Jha, A.K. Bhoi, V. Gupta, and B. Prasad, "Theoretical Analysis of the Electrical and Optical Properties of ZnS," In: A. Konkani, R. Bera, and S. Paul, editors, *Advances in Systems, Control and Automation. Lecture Notes in Electrical Engineering*, vol. 442. (Springer, Singapore, 2018). https://doi.org/10.1007/978-981-10-4762-6_2
[28] Y.L. Su, Q.Y. Zhang, N. Zhou, C.Y. Ma, X.Z. Liu, and J.J. Zhao, "Study on Co-doped ZnO comparatively by fi rst-principles calculations and relevant experiments," **250**, 123-128 (2017). https://doi.org/10.1016/j.ssc.2016.12.002
[29] T. Kato, J. L. Wu, Y. Hirai, H. Sugimoto, and V. Bermudez, "Record Efficiency for Thin-Film Polycrystalline Solar Cells Up to 22.9% Achieved by Cs-Treated Cu(In,Ga)(Se,S)$_2$," IEEE J. Photovoltaics, **9**(1), 325-330 (2019). https://doi.org/10.1109/JPHOTOV.2018.2882206
[30] A. Bouzidi, and I. Bouchama, "Numerical study of the buffer influence on the Cu(In,Ga)Se$_2$ solar cells performances by SCAPS-ID," in: International Conference on Electronics and New Technologies (ICENT), 2017.
[31] S.K. Gupta, S. Kumar, and S. Auluck, "Structural, electronic and optical properties of high pressure stable phases of ZnTe," Phys. B Condens. Matter, **404**(20), 3789-3794 (2009). https://doi.org/10.1016/j.physb.2009.06.149
[32] R. Tala-Ighil Zaïr, C. Oudjehani, and K. Tighilt, "SCAPS Simulation for Perovskite Solar Cell," J. Sol. Energy Res. Updat. **8**, 21-26 (2021). https://doi.org/10.31875/2410-2199.2021.08.3
[33] H.I. Abdalmageed, M. Fedawy, and M.H. Aly, "Effect of absorber layer bandgap of CIGS-based solar cell with (CdS/ZnS) buffer layer," J. Phys. Conf. Ser. **2128**(1), (2021). https://doi.org/10.1088/1742-6596/2128/1/012009
[34] C. Platzer-Björkman, J. Kessler, and L. Stolt, "Analysis of Zn(O,S) films for Cu(In,Ga)Se$_2$ solar cells," Proc. Estonian Acad. Sci. Phys. Math. **52**(3), 299-307 (2003). https://doi.org/10.3176/phys.math.2003.3.06
[35] Y.-K. Liao et al., "A look into the origin of shunt leakage current of Cu(In, Ga)Se$_2$ solar cells via experimental and simulation methods," Sol. Energy Mater. Sol. Cells, **117**, 145-151 (2013). https://doi.org/10.1016/j.solmat.2013.05.031
[36] P. Srivastava *et al.*, "Theoretical study of perovskite solar cell for enhancement of device performance using SCAPS-1D," Phys. Scr. 97(2), 12 (2022). https://doi.org/10.1088/1402-4896/ac9dc5
[37] M. Safari, Z. Izadi, J. Jalilian, I. Ahmad, and S. Jalali-Asadabadi, "Metal mono-chalcogenides ZnX and CdX (X = S, Se and Te) monolayers: Chemical bond and optical interband transitions by first principles calculations," Phys. Lett. Sect. A Gen. At. Solid State Phys. **381**(6), 663-670 (2017). https://doi.org/10.1016/j.physleta.2016.11.040
[38] H. T. Ganem, and A. N. Saleh, "The effect of band offsets of absorption layer on CNTS/ZnS/ZnO solar cell by SCAPS-1D," Tikrit Journal of Pure Science, **25** (6), 79-87 (2020). http://dx.doi.org/10.25130/tjps.25.2020.114
[39] N. Adim, M. Caid, D. Rached, and O. Cheref, "Computational study of structural, electronic, magnetic and optical properties of (ZnTe)m/(MnTe) n superlattices," Journal of Magnetism and Magnetic Materials, **499**, 166314 (2020). https://doi.org/10.1016/j.jmmm.2019.166314 jstor

## AB-INITIO ДОСЛІДЖЕННЯ СТРУКТУРНИХ, ЕЛЕКТРОННИХ ТА ОПТИЧНИХ ВЛАСТИВОСТЕЙ ZnX (X = Te, S і O): ЗАСТОСУВАННЯ ДО СОНЯЧНИХ БАТАРЕЙ

**Файза Бенлахдар[a], Ідріс Бушама[b,c], Тайєб Чіхі[c,d], Ібрагім Гебулі[c,d], Мохамед Амін Гебулі[c], Зохра Зерругуі[e], Кеттаб Хатір[f], Мохамед Алам Сайєд[g]**

*[a]Кафедра електроніки, технологічний факультет, Університет Сетіфа 1, 19000, Алжир*
*[b]Кафедра електроніки, технологічний факультет, Університет Мсіла, Мсіла, 28000, Алжир*
*[c]Дослідницький відділ нових матеріалів (RUEM), Університет Ферхат Аббас із Сетіфа 1, Сетіф, 19000, Алжир*
*[d]Лабораторія розробки нових матеріалів і характеристик (LENMC), Університет Ферхата Аббаса, Сетіф 19000, Алжир*
*[e]Лабораторія досліджень поверхонь і розділу твердих матеріалів (LESIMS), Департамент технологій, Ферхат АББАС Сетіфський університет, Сетіф, Алжир*
*[f]Кафедра електротехніки, технологічний факультет, Університет Мсіла, Мсіла, 28000, Алжир*
*[g]Департамент фізики, Відділ науки та технологій, Педагогічний університет, Лахор, Пакистан*

Метою роботи є дослідження структурних, електронних і оптичних властивостей сполук ZnX, зокрема тих, у яких X = Te, S і O, які мають пряму заборонену зону, що робить їх оптично активними. Щоб краще зрозуміти ці сполуки та їхні пов'язані властивості, ми провели детальні розрахунки за допомогою теорії функціоналу щільності (DFT) і програми CASTEP, яка використовує узагальнене градієнтне наближення (GGA) для оцінки функції крос-кореляції. Наші результати щодо модуля ґратки, ширини забороненої зони та оптичних параметрів узгоджуються як з експериментальними даними, так і з теоретичними прогнозами. Енергетична заборонена зона для всіх сполук є відносно великою через збільшення s-станів у валентній зоні. Наші результати показують, що оптичний перехід між (O - S - Te) - p-станами у найвищій валентній зоні та (Zn - S - O) - s-станами в нижчій зоні провідності зміщується до нижчої енергетичної зони. Таким чином, сполуки ZnX (X = Te, S і O) є перспективним варіантом для оптоелектронних пристроїв, таких як матеріали для сонячних елементів.

**Ключові слова:** *ZnTe; ZnS; ZnO; CASTEP; DFT; щільність стану; оптичні властивості*